Available online at www.sciencedirect.com

SCIENCE DIRECT

Surface & Coatings Technology 200 (2006) 2686–2694

SURFACE & COATINGS TECHNOLOGY

www.elsevier.com/locate/surfcoat

Numerical investigation on laser transformation hardening with different temporal pulse shapes

W. Wu*, N.G. Liang, C.H. Gan, G. Yu

State Key Laboratory of Nonlinear Mechanics, Institute of Mechanics, Chinese Academy of Sciences, No. 15 Beisihuanxi Road, Beijing 100080, China

Received 25 June 2004; accepted in revised form 8 November 2004
Available online 20 December 2004

Abstract

A 3-D numerical model for pulsed laser transformation hardening (LTH) is developed using the finite element method. In this model, laser spatial and temporal intensity distribution, temperature-dependent thermophysical properties of material, and multi-phase transformations are considered. The influence of laser temporal pulse shape on connectivity of hardened zone, maximum surface temperature of material and hardening depth is numerically investigated at different pulse energy levels. Results indicate that these hardening parameters are strongly dependent on the temporal pulse shape. For the rectangular temporal pulse shape, the temperature field obtained from this model is in excellent agreement with analytical solution, and the predicted hardening depth is favorably compared with experimental one. It should be pointed out that appropriate temporal pulse shape should be selected according to pulse energy level in order to achieve desirable hardening quality under certain laser spatial intensity distribution.
© 2004 Elsevier B.V. All rights reserved.

Keywords: Laser transformation hardening; Numerical modelling; Temporal pulse shape

1. Introduction

Laser transformation hardening (LTH) is an advanced heat treatment method to obtain hard, wear resistant layer on surface without affecting the bulk material through the interaction of laser and material. Compared to conventional methods, it has advantages such as low thermal distortion, less post-treatment work, good controllability of laser heat source and adaptability to geometry of component, etc. [1]. Moreover, it has been indicated that the hardened zone produced by LTH further contributes to increasing hardness, improving wear and corrosion resistance, and enhancing fatigue strength [2–5]. Usually, the hardening depth is anticipated to be as deep as possible under certain conditions.

Many approaches [6–11] have been applied to modelling continuous LTH, most of which concentrate on obtaining the quasi-steady temperature distribution of material to predict the hardening parameters. When laser beam diameter is large compared to the region of interest or the scanning velocity is appropriate, these models can make good predictions [12].

With the development of laser integrated and automatic control systems, a novel technique that treats material surface spot by spot with a pulsed laser has been developed, which makes use of the spatial and temporal shape of laser pulse to obtain ideal hardening quality [12–14]. Different from continuous LTH, laser pulse remains static or moves very slowly with respect to workpiece during pulsed laser material interaction. It is necessary to take into account the transient behavior, pulse pattern and temporal intensity distribution for simulating the pulsed laser hardening process.

The influence of laser temporal pulse shape on material drilling and welding processes has been investigated in Refs. [15–18]. Fewer works focus on the influence of temporal shape on pulsed LTH. In the present paper, a 3-D finite element model for pulsed LTH is suggested, in which laser spatial and temporal intensity distribution, temperature-dependent thermophysical properties of material, and multi-phase transformations are considered. The influence

* Corresponding author. Tel.: +86 10 62545533 3182; fax: +86 10 62579511.
E-mail address: wuwei@lnm.imech.ac.cn (W. Wu).

0257-8972/$ - see front matter © 2004 Elsevier B.V. All rights reserved.
doi:10.1016/j.surfcoat.2004.11.011

of laser temporal pulse shape on connectivity of hardened zone, maximum surface temperature of material and hardening depth is numerically investigated at different pulse energy levels. For the rectangular temporal pulse shape, the temperature field and hardening depth calculated using the current method are compared with analytical and experimental ones, respectively.

2. Hardening process induced by laser irradiation

When laser irradiates the surface of metallic material such as steel and cast iron, photons interact with electrons in the conduction band and are absorbed [19,20]. During this process, a fraction of the energy is reflected through the excited electrons transmitting photons in the form of electromagnetic waves, and the rest changes into heat energy through successive collisions between electrons and lattice phonons [1,20] before reaching equilibrium state through relaxation process [21]. The relaxation time in metals is of the order of 10^{-13} s [21] and the laser pulse duration used in this paper is of the order of 10^{-3} s. Hence, the classical Fourier's law of heat conduction can still describe this heating process. The absorption depth of laser is of the order of its wavelength [22]. In the present study, the dimensions of the hardened zones are of the order of hundred microns and the wavelength of the ND:YAG laser used is 1.06 μm, so that the laser pulse can be considered as plane heat source.

At room temperature, steel is mainly the mixture of ferrite and pearlite, while cast iron is chiefly composed of ferrite, pearlite, cementite and graphite. When appropriate laser pulse is exerted on the surface of steel or cast iron, the local temperature will rapidly be in excess of austenitizing temperature and below the melting point. In this heating course, the pearlite or ferrite will transform into austenite. When laser pulse does not irradiate, the austenite will rapidly cool down due to the surrounding material acting as an efficient heat sink, resulting in the hardening phase transformations. Consequently, a hard surface region, mainly composed of martensite, is thus produced while desirable bulk properties, such as toughness and ductility, remain almost unaffected. Such a process is called 'self-quenching'.

3. Numerical model

Heat conduction plays an important role in pulsed LTH. As mentioned above, the classical Fourier's law of heat conduction can be used to describe the current laser surface treatment and the equation of heat conduction takes the form

$$\rho c\frac{\partial T}{\partial t} = \nabla\cdot(k\nabla T) + \rho\dot{Q}, \tag{1}$$

where ρ is the material density, c the specific heat, k the thermal conductivity and $\dot{Q}$ the rate of internal energy generation of per unit mass.

It has been pointed out [6] that the heat energy losses due to convection and radiation can be neglected during LTH. Therefore, only two kinds of boundary conditions need to be treated, i.e., specified temperature $T=T(\Gamma_1, t)$ on boundary Γ_1 and specified heat flux $q=q(\Gamma_2, t)$ on boundary Γ_2, where $\Gamma_1+\Gamma_2=\Gamma_{\text{total}}$ (entire boundary). The initial condition is $T=T_0$ (x, y, z).

Phase transformation will proceed under a nonequilibrium state due to the rapidity of heating and cooling during LTH, which indicates that phase transformation occurs over a temperature range rather than at a constant temperature. In this case, the latent heat can be treated as equivalent specific heat. When phase transformation takes place, the released or absorbed heat quantity, Q, is proportional to the fraction transformed, V, and V is the function of temperature, T. Then, the second term on the right of Eq. (1) can be rewritten as

$$\rho\dot{Q} = -\rho\frac{\partial Q}{\partial t} = -\rho\frac{\partial Q}{\partial V}\frac{\partial V}{\partial T}\frac{\partial T}{\partial t} = -\rho c_{\text{eq}}\frac{\partial T}{\partial t}, \tag{2}$$

with

$$c_{\text{eq}} = \frac{\partial Q}{\partial V}\frac{\partial V}{\partial T}, \tag{3}$$

where c_{eq} is defined as equivalent specific heat. Marking $\overline{c}=c+c_{\text{eq}}$ and substituting Eq. (2) into Eq. (1), one can get

$$\rho\overline{c}\frac{\partial T}{\partial t} = \nabla\cdot(k\nabla T). \tag{4}$$

For different type of phase transformation, the equivalent specific heat can be drawn depending on the corresponding regularity of phase transformation.

For diffusion-controlled phase transformation such as austenite-to-pearlite reaction, Avrami Equation [23] describes the relationship between the fraction transformed, V, and isothermal transformation time, t, i.e.,

$$V = 1 - \exp(-Bt^n), \tag{5}$$

where B and n are material parameters and can be calculated as follows:

$$n = \frac{\ln\left[\dfrac{\ln(1-V_1)}{\ln(1-V_2)}\right]}{\ln\frac{t_1}{t_2}}, \quad B = -\frac{\ln(1-V_1)}{t_1^n}, \tag{6}$$

where t_i and V_i $(i=1, 2)$ are isothermal transformation time and corresponding fraction transformed at certain temperature, respectively, and can be measured according to T–T–T diagrams.

In the present work, Eq. (5) is applied under continuous cooling conditions as done by Scheil [24,25]. It is implemented by subdividing the cooling curve into a series of isothermal time steps and calculating the fraction of incubation period consumed in each step. This approach is schematically demonstrated in Fig. 1, where Δt_i is the ith time step, t_{T_i} the incubation period at temperature T_i, t_s the starting time of transformation, t_e the ending time of transformation, T_s the starting temperature of transformation, and T_e the ending temperature of transformation. When $\Sigma\Delta t_i/t_{T_i}=1$, the transformation starts. Denote V_i the fraction

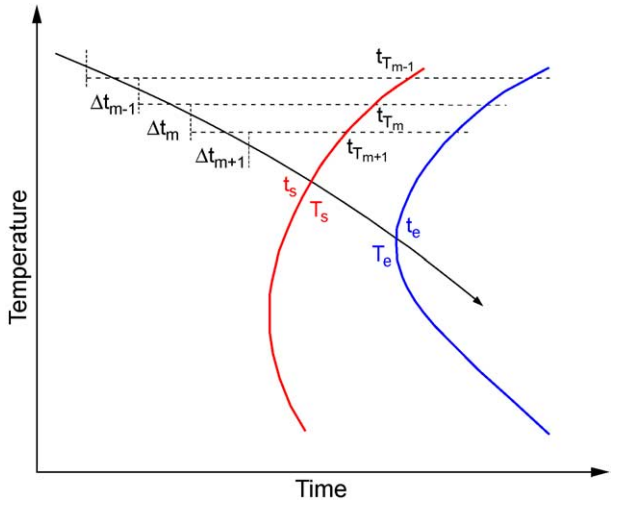

Fig. 1. Schematic diagrams of dealing with continuous cooling conditions.

transformed during the ith time step at temperature T_i. The fraction transformed, V_{i+1}, during the $(i+1)$th time step at temperature T_{i+1} can thus be expressed as

$$V_{i+1} = 1 - \exp[-B_{i+1}(t^*_{i+1} + \Delta t_{i+1})^{n_{i+1}}], \tag{7}$$

with

$$t^*_{i+1} = \left[-\frac{\ln(1-V_i)}{B_{i+1}}\right]^{\frac{1}{n_{i+1}}}, \tag{8}$$

where t^*_{i+1} is called virtual time [25,26]. The increment of fraction transformed over the time interval, ΔV, is then $V_{i+1}-V_i$. The variation of heat quantity, ΔQ, is proportional to ΔV, and can be expressed as

$$\Delta Q = \rho L \Delta V, \tag{9}$$

where L denotes latent heat of per unit mass.

For diffusion-free phase transformation such as austenite-to-martensite reaction, the fraction transformed, V, is calculated from the empirical equation proposed by Koistinen and Marburger [27]:

$$V = 1 - \exp[-0.011(M_s - T)], \tag{10}$$

where M_s is the martensite start temperature, T the instantaneous temperature. When the temperature varies from T_i to T_{i+1}, the increment of martensite volume fraction, ΔV, can be obtained by using Eq. (10). The variation of heat quantity, ΔQ, takes the same form as Eq. (9).

In some cases, melting and solidification may take place during LTH. Therefore, the latent heat of fusion should be considered in calculation. The volume fraction of melting or solidification, V, can be linearly written as the function of temperature, T:

$$V = \frac{T - T_s}{T_e - T_s}, \tag{11}$$

where T_s and T_e are the starting and ending temperature of transformation, respectively. When phase transformation occurs, the increment of fraction transformed, ΔV, can be determined by using Eq. (11). The variation of heat quantity, ΔQ, can also be calculated from Eq. (9).

When temperature varies from T_n to T_{n+1}, applying equivalent relation of heat quantity yields

$$\Delta Q + \rho c(T_{n+1} - T_n) = \rho \bar{c}\,(T_{n+1} - T_n). \tag{12}$$

By substituting $\bar{c}=c+c_{eq}$ and Eq. (9) into Eq. (12), the equivalent specific heat can be derived as follows:

$$c_{eq} = \frac{L\Delta V}{T_{n+1} - T_n}. \tag{13}$$

The six possibilities for two successive states in a step of temperature varying from T_n to T_{n+1} are shown in Fig. 2. The equivalent specific heat of the six cases can be obtained by calculating the corresponding increment of volume fraction transformed, ΔV, respectively. Particularly, the corresponding values of the six cases for melting or solidification can be determined as follows:

$$c_{eq} = \begin{cases} 0 & \text{Cases(1) and (2)}, \\ \frac{T_{n+1}-T_s}{T_{n+1}-T_n}\cdot\frac{L}{T_e-T_s} & \text{Case(3)}, \\ \frac{L}{T_e-T_s} & \text{Case(4)}, \\ \frac{T_e-T_n}{T_{n+1}-T_n}\cdot\frac{L}{T_e-T_s} & \text{Case(5)}, \\ \frac{L}{T_{n+1}-T_n} & \text{Case(6)}. \end{cases} \tag{14}$$

In practical calculation, when case (6) occurs, the current time step will be bisected to ensure the computational reliability.

In finite element analysis, the unknown temperature, T, is usually written as

$$T = \sum_{j=1}^{n} N_j(x,y,z)T_j(t), \tag{15}$$

where T_j is nodal temperature and N_j is shape function. By applying a Galerkin weighted residual process, Eq. (4) with

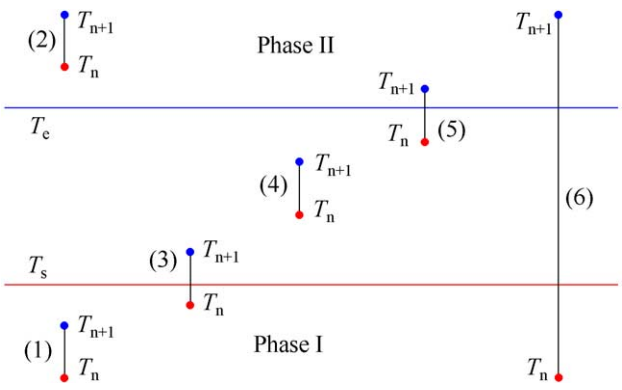

Fig. 2. Six possibilities of temperature variation.

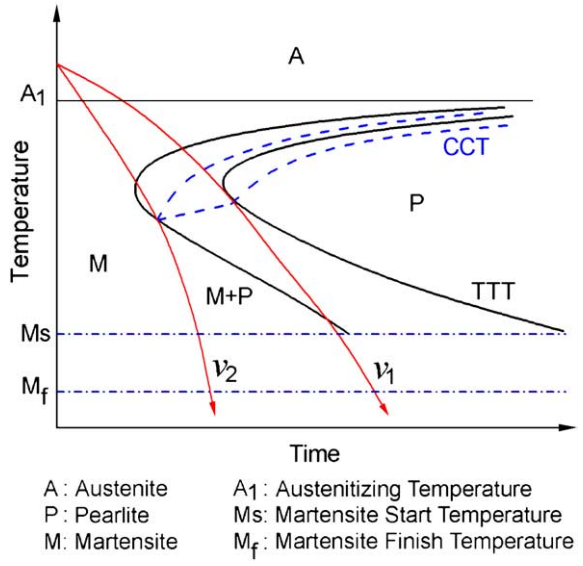

Fig. 3. Schematic diagrams of phase transformations when cooling.

boundary conditions $T=T(\Gamma_1, t)$ and $k\partial T/\partial n+q(\Gamma_2, t)=0$ is expressed as

$$\boldsymbol{C}\dot{\boldsymbol{T}} + \boldsymbol{K}\boldsymbol{T} + \boldsymbol{P} = 0, \tag{16}$$

where $\boldsymbol{C}$, $\boldsymbol{K}$ and $\boldsymbol{P}$ are heat capacity matrix, heat conduction matrix and vector of applied heat loads, respectively. The elements of the matrices and vector are

$$C_{ij} = \sum \int_{\Omega^e} \rho \bar{c} N_i N_j \mathrm{d}\Omega^e, \tag{17}$$

$$K_{ij} = \sum \int_{\Omega^e} \left(k_x \frac{\partial N_i}{\partial x}\frac{\partial N_j}{\partial x} + k_y \frac{\partial N_i}{\partial y}\frac{\partial N_j}{\partial y} + k_z \frac{\partial N_i}{\partial z}\frac{\partial N_j}{\partial z} \right) \mathrm{d}\Omega^e, \tag{18}$$

$$P_i = \sum \int_{\Gamma_2^e} q N_i \mathrm{d}\Gamma_2^e. \tag{19}$$

Here, only a brief procedure of finite element analysis is presented. The details of numerical scheme are available in Ref. [28]. By incorporating Eq. (16) with microstructural evolution rule, the hardening parameters such as connectivity of hardened zone, maximum surface temperature and hardening depth can be identified.

As described earlier, the surrounding material will assist the cooling of the austenite after laser pulse moving away. According to cooling velocity, v, austenite will transform into different phases such as pearlite, bainite and martensite, etc. In this paper, the simplified microstructural evolution rule is used as illustrated in Fig. 3, where v_1 and v_2 are lower and upper critical cooling velocity, respectively. From the figure, it can be seen that (1) if $v<v_1$, austenite will transform into pearlite; (2) if $v>v_2$ and temperature $T<M_s$, austenite will transform into martensite; and (3) if $v_1 \le v \le v_2$, austenite will partially transform into pearlite, and the rest will transform into martensite when $T<M_s$.

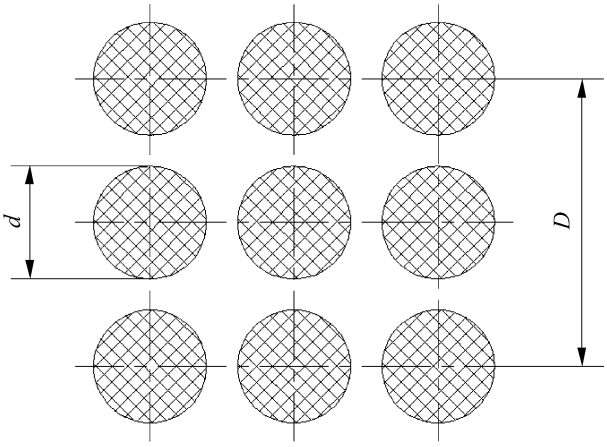

Fig. 4. Sketch of point-Type-pattern of laser pulse.

4. Laser-material parameters and finite element mesh

In the present study, a ND:YAG laser of a wavelength 1.06 μm is used. The raw laser beam has been transformed into a point-Type-pattern before nine spots simultaneously irradiating material surface as shown in Fig. 4, where d=0.36 mm and D=0.8 mm. The uniformly spatial intensity distribution of laser pulse is adopted and the pulse duration is 24 ms.

The three types of laser temporal pulse shapes are adopted as shown in Fig. 5, where P is laser power intensity, τ_0 pulse duration and τ the parameter that governs the temporal pulse shape. 'A-Type', 'B-Type' and 'C-Type' denote the three cases of temporal pulse shape varying with τ, respectively. When τ=0, temporal pulse shape is a rectangle, which implies that P keeps constant. When

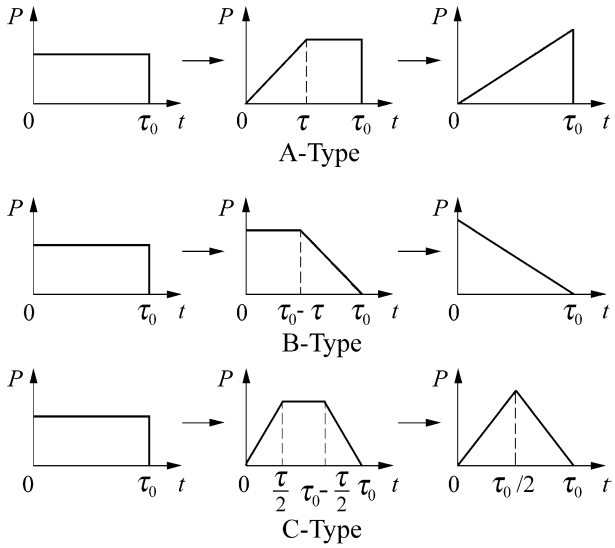

Fig. 5. Laser temporal pulse shapes.

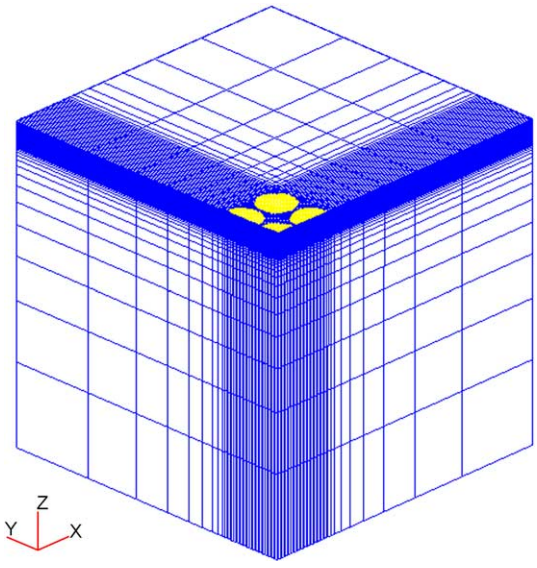

Fig. 6. 3-D finite element mesh.

$\tau=\tau_0$, A-Type is the case that P linearly increases from zero to peak value, B-Type the case that P linearly decreases from peak value to zero, and C-Type the case that P linearly increases from zero to peak value first, then linearly decreases from peak value to zero. For every type, apparently, the peak power intensity will vary with τ when pulse energy keeps constant.

A kind of pearlitic ductile iron QT70 having a composition of 3.3% wt C, 2.15% wt Si, 1.0% wt Ni and 0.6% wt Mn is selected for the present study and the related thermophysical parameters are found in Refs. [29–33]. The average absorptivity of the material to the ND:YAG laser is measured to be ~0.25.

Only 1/4 of the workpiece needs to be computed because of the symmetry. The corresponding 3-D finite element mesh locally refined is plotted in Fig. 6, where 8-node-hexahedron element is adopted. Size of the mesh is large enough to simulate infinite conditions. On the region laser pulse irradiating, specified heat flux boundary conditions are given. On the symmetrical surfaces and the region without laser acting upon of the top face, adiabatic boundary conditions are adopted. On the other boundaries, specified temperature conditions are prescribed. The initial temperature is the room temperature 25 °C.

5. Results and discussions

The influence of laser temporal pulse shape on connectivity of hardened zone, maximum surface temperature

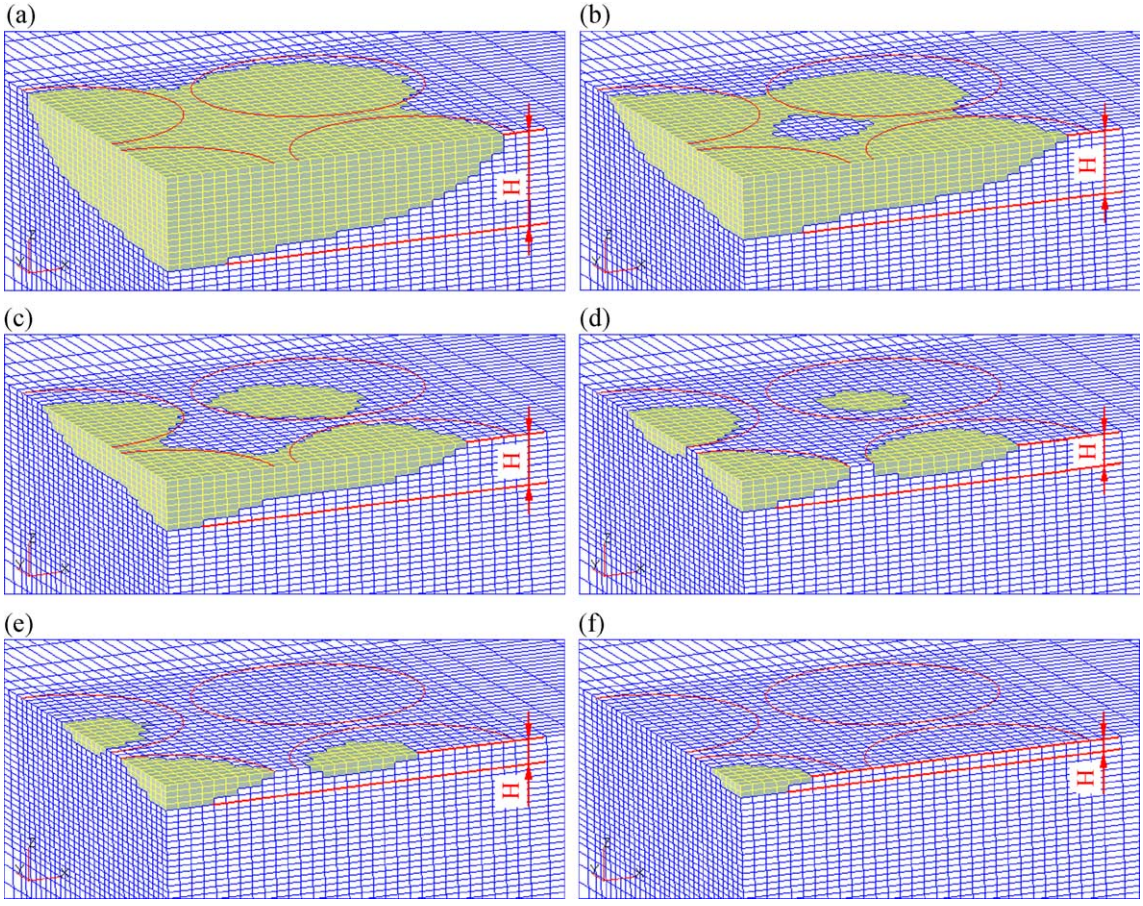

Fig. 7. Several typical shapes of hardened zone.

Table 1a
Shapes of hardened zone produced by A-Type

E^*	t^*										
	0	0.1	0.2	0.3	0.4	0.5	0.6	0.7	0.8	0.9	1.0
0.875	f	f	e	e	d	c	c	c	c	b	b
1.0	e	c	c	c	b	b	b	b	b	b	b
1.25	b	b	a	a	a	a	a	a	a	a	a
1.5	a	a	a	a	a	a	a	a	a	a	a

Table 1c
Shapes of hardened zone produced by C-Type

E^*	t^*										
	0	0.1	0.2	0.3	0.4	0.5	0.6	0.7	0.8	0.9	1.0
0.875	f	f	f	e	e	d	d	c	c	c	c
1.0	e	c	c	c	c	b	b	b	b	b	b
1.25	b	b	a	a	a	a	a	a	a	a	a
1.5	a	a	a	a	a	a	a	a	a	a	a

and hardening depth is studied by using the above model. Dimensionless terms $E^*=E/E_0$, $T^*_{max}=T_{max}/T_m$, $H^*=H/H_0$ and $t^*=\tau/\tau_0$ are used. E is per laser pulse energy and E_0=8 J. T_{max} is maximum surface temperature and T_m is melting point of material. H is hardening depth and H_0 is the hardening depth produced by the rectangular temporal pulse shape when pulse energy is E_0. Parameters τ and τ_0 have been described in Section 4.

The several typical shapes of hardened zone are shown in Fig. 7, where the hardening depth, H, is defined as the maximum depth of hardened layer. In the area irradiated by each laser spot shown in Fig. 4, hardened piece may be produced during pulsed LTH. In this paper, the connectivity of hardened zone refers to the degree of connection between the hardened pieces. From Fig. 7a–f, the connectivity of hardened zone decreases in turn. When τ varies, the shapes of hardened zone at various energy levels are listed in Tables 1a–1c, where the letters, 'a'–'f', correspond with the shapes of hardened zone shown in Fig. 7, respectively. From the tables, it can be seen that the connectivity of hardened zone gradually increases with τ when E keeps constant, or with E when τ keeps constant. It can also be seen that the hardened zone produced by A-Type has better connectivity than those generated by the other temporal shapes when E and τ are given.

As mentioned before, a region is possibly hardened only when the temperature is high enough to form austenite during LTH. In some cases, the maximum temperature of the regions between laser spots or the regions irradiated by spots away from center does not exceed the austenitizing temperature. Consequently, the hardened layer will not be produced in these regions. For example, in Fig. 7, b–d denote the cases that the regions between laser spots are not hardened, while e and f represent the cases that the regions irradiated by laser spots away from center are not hardened. It is just because of the different temperature distributions caused by heat conduction that the hardened zone shapes exhibit diversity when temporal shape or pulse energy varies.

Table 1b
Shapes of hardened zone produced by B-Type

E^*	t^*										
	0	0.1	0.2	0.3	0.4	0.5	0.6	0.7	0.8	0.9	1.0
0.875	f	f	f	e	e	e	e	e	e	e	e
1.0	e	d	c	c	c	c	c	c	c	c	c
1.25	b	b	b	a	a	a	a	a	a	a	a
1.5	a	a	a	a	a	a	a	a	a	a	a

At three energy levels, the variations of maximum surface temperature, T_{max}, and hardening depth, H, with τ are plotted in a and b in Fig. 8, respectively. The figure shows that there exists good correlation between T_{max} and H. For A-Type, T_{max} almost linearly depends on τ. For B-Type, T_{max} increases first, then gradually tends to be stable as τ increases. For C-Type, the increasing τ gives a rising tendency of T_{max} with gradually dropping amplitudes.

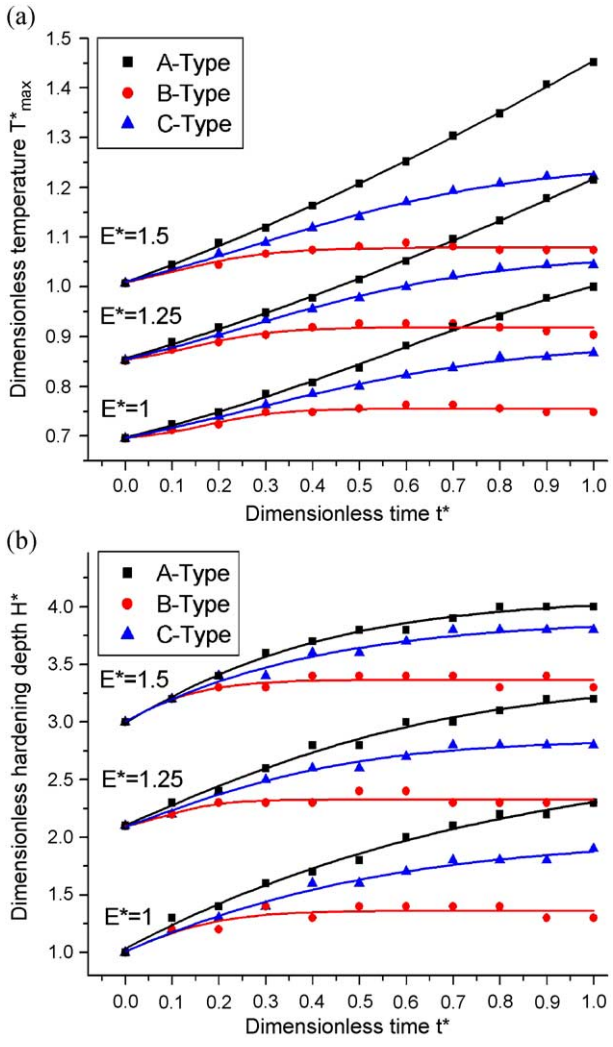

Fig. 8. Variations of maximum surface temperature (a) and hardening depth (b) with parameter τ at different energy levels.

The variations of H are analogous to those of T_{max}, yet H increases slowly with τ due to the effect of latent heat of fusion under the action of A-Type at higher energy levels. When τ is given at every pulse energy level, Fig. 8 also shows that A-Type generates higher T_{max} and thicker hardened layer than those produced by the other types, and B-Type produces the minimum ones.

When laser irradiates material surface, a fraction of the incident laser energy will change into heat energy and diffuse into material through heat conduction. When heat inflow is more than heat outflow, temperature will go up. Conversely, temperature will go down.

For A-Type, laser power gradually increases from zero to its peak value, which implies that the energy absorbed by material per unit time never decreases before laser pulse moving away. When pulse duration τ_0 is specified, the peak power and T_{max} will increase with the increase of τ. Correspondingly, H will increase.

For B-Type, laser power gradually decreases from peak value to zero. The energy absorbed by material per unit time never increases during pulse irradiating. When the absorbed energy cannot compensate the losses caused by heat conduction, temperature will go down. It implies that surface temperature should reach its maximum value when laser pulse still works. Although the peak power continuously increases as τ increases, the duration time of laser working at peak power gradually decreases. This is the reason why T_{max} varies in the way shown in Fig. 8a. As a result of temperature field evolution, H should vary in a similar way just as plotted in Fig. 8b.

For C-Type, laser power gradually reaches its peak value from zero, and keeps for a while. After that, it gradually decreases to zero. This type can be regarded as the combination of A-Type and B-Type, which implies that T_{max} and H vary with τ under the action of C-Type are between A-Type and B-Type. Just as shown in Fig. 8, T_{max} and the corresponding H increase with gradually dropping amplitudes.

Although the variations of T_{max} or H with τ are similar at every pulse energy level, the choice of temporal pulse shape is different for practical pulsed LTH. The prerequisite for selecting temporal pulse shape is how to make hardening depth be maximum with material surface no-or-slightly melting under certain laser spatial intensity distribution and pulse energy. For example, Fig. 8 demonstrates that A-Type with t^*=1.0 should be selected when E^*=1.0, A-Type with t^*=0.5 or C-Type with t^*=0.6–0.7 should be adopted when E^*=1.25, and the rectangular temporal pulse shape should be used when E^*=1.5.

When T_{max} or H is given, the variation of requested pulse energy E with τ is shown in a and b in Fig. 9, respectively. It can be seen that the requested E strongly depends on temporal pulse shape. For A-Type, the requested E gradually decreases with the increase of τ. For B-Type, the requested E decreases in the beginning, then gradually tends to be constant as τ increases. For C-Type, the variation of requested E is similar to that under the action of A-Type, but decreases more slowly. When τ is given, apparently, the requested E of A-Type is minimum. For certain pulse energy, it can be inferred that hardened layer may not be produced by using rectangular temporal pulse shape, whereas it can be obtained by adopting other temporal pulse shapes.

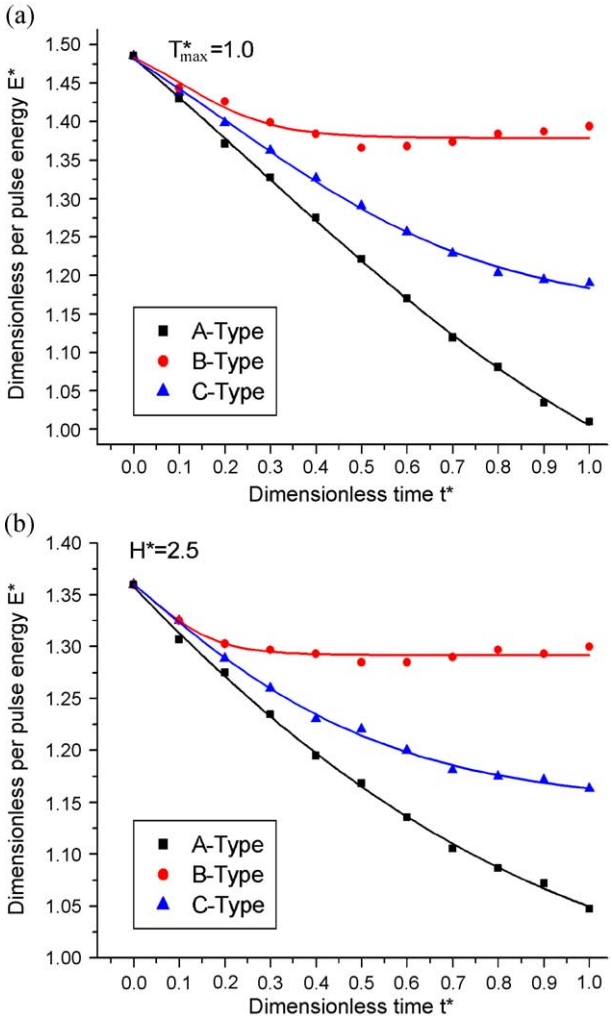

Fig. 9. Variation of per pulse energy with parameter τ when maximum surface temperature (a) or hardening depth (b) is given.

6. Accuracy assessing

In order to assess the accuracy of the numerical investigation, the temperature field obtained by the present method is compared with the analytical solution [21] for semi-infinite body subjected to a laser pulse with a spatially uniform intensity distribution and a rectangular temporal shape on the surface. The temperature-vs.-time curves at various depths are plotted in Fig. 10, where τ_0 is the pulse duration, α the material thermal diffusivity, and z^* the dimensionless depth. Results show good agreement between numerical solutions and analytical ones apart from the boundary effects.

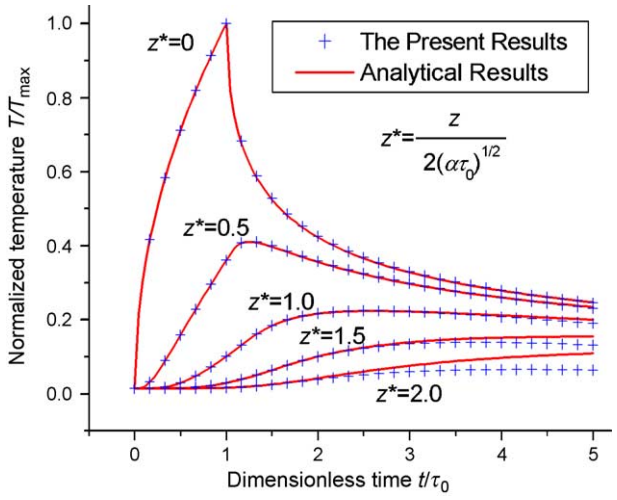

Fig. 10. Comparison between the present temperature field and analytical one.

The hardening depth predicted by the present method is also compared with experimental data. A specimen with dimensions 19×9×9 mm^3 is cut from the material QT70 described in Section 4. The raw laser beam has been transformed into the pattern shown in Fig. 4 before irradiating the specimen. The pulse energy is 12 J, and the pulse duration with a rectangular temporal shape is 24 ms. The Vickers microhardness distributions of hardened zone are shown in Fig. 11. The predicted hardening depth is 175 μm, which is favorably compared with experimental one 160–220 μm.

7. Conclusions

(1) A 3-D numerical model for pulsed LTH is established using the finite element method. In this model, laser spatial and temporal intensity distribution, temperature-dependent thermophysical properties of material, and multi-phase transformations are considered. The influence of laser temporal pulse shapes on hardening parameters such as connectivity of hardened zone, maximum surface temperature and hardening depth is investigated at different pulse energy levels. Results indicate that temporal pulse shape has great effects on these hardening parameters.

(2) When E keeps constant, the connectivity of hardened zone gradually increases with τ. When τ keeps constant, the connectivity of hardened zone gradually increases with E. When E and τ are given, the hardened zone produced by A-Type has better connectivity than those generated by the other types.

(3) For A-Type, T_{max} and H always increase with τ when E keeps constant, and the requested E always decreases as τ increases when T_{max} or H is given. For B-Type, T_{max} and H increase with τ first, then gradually tend to be stable when E keeps constant, and the requested E decreases in the beginning, then gradually tends to be constant as τ increases when T_{max} or H is given. For C-Type, the amplitudes of T_{max} and H increasing with τ are smaller than those produced by A-Type when E keeps constant, and the requested E decreases more slowly as τ increases than that produced by A-Type when T_{max} or H is given.

(4) When τ is given at every pulse energy level, A-Type generates higher T_{max} and thicker hardened layer than those produced by the other types, and B-Type produces the minimum ones. When T_{max} or H is given and τ keeps constant, the requested E of A-Type is minimum, and that of B-Type is maximum.

(5) Appropriate temporal pulse shape should be selected according to pulse energy level in order to obtain desirable hardening quality under certain laser spatial intensity distribution. For the rectangular temporal pulse shape, the temperature field and hardening depth calculated using the current method are compared with analytical and experimental ones, respectively. Results show good agreement.

Acknowledgements

This research work was sponsored by National Natural Science Foundation of China through Grant No. 10232050, and also by Ministry of Science and Technology Foundation No. 2002CB412706.

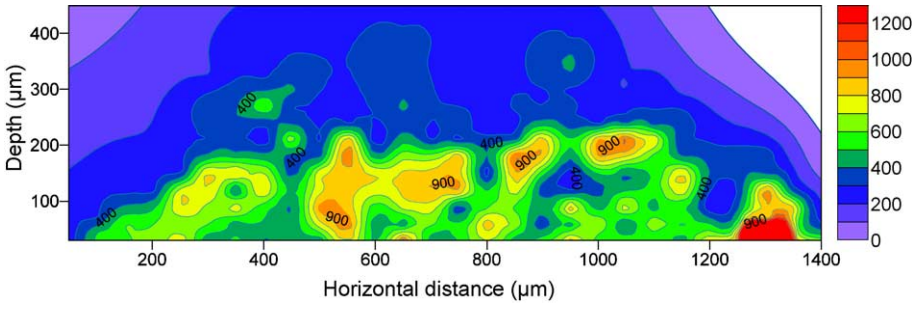

Fig. 11. Vickers microhardness distribution profile of laser hardened zone.

References

[1] W.M. Steen, Laser Material Processing, Springer, London, 1991.
[2] D.I. Pantelis, G. Pantazopoulos, S.S. Antoniou, Wear 205 (1997) 178.
[3] R. Sagaro, J.S. Ceballos, A. Blanco, J. Mascarell, Wear 225–229 (1999) 575.
[4] D.I. Pantelis, E. Bouyiouri, N. Kouloumbi, et al., Surf. Coat. Technol. 298 (2002) 125.
[5] K.H. Lo, F.T. Cheng, H.C. Man, Surf. Coat. Technol. 173 (2003) 96.
[6] S. Kou, D.K. Sun, Y.P. Le, Metall. Trans., A, Phys. Metall. Mater. Sci. 14A (1983) 643.
[7] M.F. Ashby, K.E. Easterling, Acta Metall. 32 (1984) 1935.
[8] M. Davis, P. Kapadia, J. Dowden, et al., J. Phys., D, Appl. Phys. 19 (1986) 1981.
[9] J.C. Ion, H.R. Shercliff, M.F. Ashby, Acta Metall. Mater. 40 (1992) 1539.
[10] R. Komanduri, Z.B. Hou, Int. J. Heat Mass Transfer 44 (2001) 2845.
[11] V. Colombo, A. Mentrelli, T. Trombetti, Eur. Phys. J., D At. Mol. Opt. Phys. 27 (2003) 239.
[12] P.R. Woodard, J. Dryden, J. Appl. Phys. 85 (1999) 2488.
[13] J.C. Ion, Surf. Eng. 18 (2002) 14.
[14] G. Yu, H.J. Yu, Integrated Laser Intelligent Manufacturing, Metallurgic Industry Press, Beijing, 2002 (in Chinese).
[15] S.O. Roos, J. Appl. Phys. 51 (1980) 5061.
[16] P.S. Mohanty, A. Kar, J. Mazumder, J. Laser Appl. 8 (1996) 291.
[17] L. Grad, J. Možina, Appl. Surf. Sci. 127–129 (1998) 999.
[18] D.K.Y. Low, L. Li, P.J. Byrd, Opt. Lasers Eng. 35 (2001) 149.
[19] D. Bäuerle, Laser Processing and Chemistry, third edition, Springer-Verlag, Berlin, 2000.
[20] B.S. Yilbas, Int. J. Eng. Sci. 24 (1986) 1325.
[21] M. von Allmen, Laser-Beam Interactions with Materials—Physical Principles and Applications, Springer-Verlag, Berlin, 1987.
[22] L. Migliore (Ed.), Laser Materials Processing, Marcel Dekker, New York, 1996.
[23] M. Avrami, J. Chem. Phys. 8 (1940) 212.
[24] D. Hömberg, Acta Mater. 44 (1996) 4375.
[25] P.K. Agarwal, J.K. Brimacombe, Metall. Trans., B, Process Metall. 12B (1981) 121.
[26] E.B. Hawbolt, B. Chau, J.K. Brimacombe, Metall. Trans., A, Phys. Metall. Mater. Sci. 14A (1983) 1803.
[27] D.P. Koistinen, R.E. Marburger, Acta Metall. 7 (1959) 59.
[28] O.C. Zienkiewicz, The Finite Element Method, third edition, McGRAW-HILL Book (UK), London, 1977.
[29] Y.Q. Liu, Heat Treatment of Steel, Metallurgic Industry Press, Beijing, 1987 (in Chinese).
[30] Z. Tan, G.W. Guo, Thermophysical Properties of Engineering Alloys, Metallurgic Industry Press, Beijing, 1994 (in Chinese).
[31] Z.Z. Hu, Handbook of Steels and Heat Treatment Curves, National Defence Industry Press, Beijing, 1986 (in Chinese).
[32] Z.G. Zhao, L.W. Zhang, Z.B. Zhang, et al., J. Dalian Univ. Technol. 35 (1995) 164 (in Chinese).
[33] E.A. Brandes (Ed.), Smithells Metals Reference Book, sixth edition, Butterworth & Co (Publishers), London, 1983.